

# A geometrical view of scalar modulation instability

S. M. Hernandez<sup>1,\*</sup>, P. I. Fierens<sup>2,3</sup>, J. Bonetti<sup>1</sup>, A. D. Sánchez<sup>1</sup>,  
and D. F. Grosz<sup>1,3</sup>

<sup>1</sup>Grupo de Comunicaciones Ópticas, Instituto Balseiro, Bariloche,  
Río Negro 8400, Argentina

<sup>2</sup>Grupo de Optoelectrónica, Instituto Tecnológico de Buenos  
Aires, CABA 1106, Argentina

<sup>3</sup>Consejo Nacional de Investigaciones Científicas y Técnicas  
(CONICET), Argentina

\*Corresponding author: shernandez@ib.edu.ar

March 1, 2022

## Abstract

We present a novel approach to the analysis of a full model of scalar modulation instability (MI) by means of a simple geometrical description in the power vs. frequency plane. This formulation allows to relate the shape of the MI gain to any arbitrary dispersion profile of the medium. As a result, we derive a straightforward explanation of the non-trivial dependence of the cutoff power on high-order dispersion and obtain explicitly the power that maximizes the gain. Our approach puts forth a powerful tool to synthesize a desired MI gain with the potential application to a vast number of parametric-amplification and supercontinuum-generation devices whose functioning relies upon modulation instability.

## 1 Introduction

The phenomenon of modulation instability (MI) has been known and thoroughly studied for many years in a vast number of different areas of science. In the realm of optical fibers [1, 2, 3, 4, 5, 6, 7], MI plays a fundamental role as it is intimately connected to the appearance of optical solitons, which have had a strong impact on applications to high-capacity fiber-optic communication, among other areas. Modulation instability also is at the heart of the occurrence of efficient parametric optical processes heavily relied upon to achieve bright and coherent light in various spectral ranges. These very same nonlinear processes are used

to provide optical amplification and wavelength conversion in the telecommunication band, maybe one day enabling complete photonic control of optical data traffic. In recent years, nonlinear phenomena such as supercontinuum generation [8, 9, 10, 11, 12] and rogue waves [13, 14, 15] have rekindled the interest in MI.

In the present work we use a complete analysis of MI, first presented in [16] to study coherence in seeded MI, but now turning our attention to the interplay between high-order dispersion and self-steepening. By analyzing the dependence of the MI gain with pump power in this complete model including both the delayed Raman response and the effect of self-steepening, we find that self-steepening yields an optimum power (in terms of maximizing the gain) and a cutoff power above which the MI gain essentially vanishes, leaving behind only the Raman contribution. These observations regarding the power cutoff and the optimum power in the presence of self-steepening were first reported by Shukla and Rasmussen [17], and the role of self-steepening was further analyzed by De Angelis *et al.* [18]. However, in both references the effects of high-order dispersion and delayed Raman response were not considered. In this work not only we extend these results, but put forth an analysis in the pump-power-versus-frequency plane, showing that the region where MI gain exists possesses remarkably simple geometrical properties, thus providing a powerful tool for the analysis and synthesis of any arbitrary gain profile.

The remaining of the paper is organized as follows: In Section 2, we briefly review an expression for the MI gain that contemplates all relevant nonlinear effects. Section 3 is devoted to the description of the modulation instability gain in the pump-power-versus-frequency plane and introduces the geometrical model. Analytical expressions for finding gain maxima and the influence of high-order dispersion are presented in Section 4. Concluding remarks are presented in Section 5.

## 2 Analytical expression of the MI gain

Scalar wave propagation in a lossless nonlinear medium can be described by the generalized nonlinear Schrödinger equation [19],

$$\frac{\partial A}{\partial z} - i\hat{\beta}A = i\hat{\gamma}A(z, T) \int_{-\infty}^{+\infty} R(T') |A(z, T - T')|^2 dT', \quad (1)$$

where  $A(z, T)$  is the slowly-varying envelope,  $z$  is the spatial coordinate, and  $T$  is the time coordinate in a comoving frame at the group velocity ( $= \beta_1^{-1}$ ).  $\hat{\beta}$  and  $\hat{\gamma}$  are operators related to the dispersion and nonlinearity, respectively, and are defined by

$$\hat{\beta} = \sum_{m \geq 2} \frac{i^m}{m!} \beta_m \frac{\partial^m}{\partial T^m}, \quad \hat{\gamma} = \sum_{n \geq 0} \frac{i^n}{n!} \gamma_n \frac{\partial^n}{\partial T^n}.$$

The  $\beta_m$ 's are the coefficients of the Taylor expansion of the propagation constant  $\beta(\omega)$  around a central frequency  $\omega_0$ . In the convolution integral in the right hand side of (1),  $R(T)$  is the response function that includes both the instantaneous (electronic) and delayed Raman response of the medium.

The MI gain is given by (see, e.g., [16])

$$g(\Omega) = 2 \max\{-\text{Im}\{K_1(\Omega)\}, -\text{Im}\{K_2(\Omega)\}, 0\}, \quad (2)$$

where  $\Omega = \omega - \omega_0$ , and  $K_{1,2}(\Omega)$  are dispersion relations of small perturbations  $a = D \exp(iK_{1,2}(\Omega)z)$  to a continuous-wave (CW) pump of frequency  $\omega_0$  and power  $P_0$  such that  $(\sqrt{P_0} + a) e^{i\gamma_0 P_0 z}$  is an approximate solution to (1) when only linear terms on the perturbation are considered.

Then, the MI gain with all relevant nonlinear effects present in (1) can be obtained (for more details, see Ref. [16]) by finding  $K_{1,2}(\Omega)$ . In the vast majority of the literature only up to  $\gamma_1$  is taken into account. As such, we focus on a simple expression obtained by setting  $\gamma_{n \geq 2} = 0$  and  $\gamma_1 = \gamma_0 \tau_{\text{sh}}$  (accounting for the effect of self-steepening). Then,

$$K_{1,2}(\Omega) = \tilde{\beta}_o + P_0 \gamma_0 \tau_{\text{sh}} \Omega \left(1 + \tilde{R}\right) \pm \pm \sqrt{\left(\tilde{\beta}_e + 2\gamma_0 P_0 \tilde{R}\right) \tilde{\beta}_e + P_0^2 \gamma_0^2 \tau_{\text{sh}}^2 \Omega^2 \tilde{R}^2}, \quad (3)$$

with  $\tilde{R}$  the Fourier transform of  $R$ ,

$$\tilde{\beta}_e(\Omega) = \sum_{n \geq 1} \frac{\beta_{2n}}{(2n)!} \Omega^{2n}, \text{ and } \tilde{\beta}_o(\Omega) = \sum_{n \geq 1} \frac{\beta_{2n+1}}{(2n+1)!} \Omega^{2n+1}.$$

### 3 Geometry of the MI gain

Equations (2)-(3) exhibit some properties of the gain that have been thoroughly studied in the literature, for instance, the fact that it does not depend on odd terms of the dispersion relation (e.g.,  $\beta_3$ ) [4, 10]. However, the derived MI gain, including the effects of self-steepening and Raman delayed response, reveals novel aspects related to the self-steepening term  $\gamma_0 \tau_{\text{sh}}$ . Indeed, it already has been noted that this term enables a gain even in a zero-dispersion optical fiber and that, in general, leads to a narrowing of the MI gain bandwidth [20, 21]. These observations are shown to be a straightforward consequence of the analysis that follows.

It is widely known (see, e.g., Ref. [19]) that, for the simplified model that only takes  $\beta_2$  and  $\gamma_0$  into account and neglects self-steepening, as the pump power  $P_0$  increases the frequency  $\Omega_{\text{max}}$  where the MI gain attains its maximum, and the peak gain both increase as, respectively,

$$\Omega_{\text{max}} = \pm \sqrt{\frac{2\gamma_0 P_0}{|\beta_2|}}, \quad g(\Omega_{\text{max}}) = 2\gamma_0 P_0. \quad (4)$$

Enter self-steepening and the relation between the pump power and the MI gain changes drastically in a non-trivial way, since there appears an optimum pump power level for which a peak gain is attained, and any further increase in pump power makes the MI gain decline. This relevant observation was first made by Shukla and Rasmussen [17] with a simplified model of dispersion expanded up to the GVD parameter. In what follows, we find that this feature is retained when considering an arbitrary number of dispersion terms. Moreover, we show this to be a corollary of the geometrical properties of the region where MI gain occurs, as defined over the pump-power-versus-frequency plane.

To this purpose, let us analyze the case of Eq. (3) where only the electronic Raman response is taken into account (i.e.,  $\tilde{R}(\Omega) = 1$ ). With the help of some examples (cf. Fig. 2), this simplification is shown to be not too restrictive. Thus, under this setting,

$$g(\Omega, P_0) = \begin{cases} 2\sqrt{\Delta(\Omega, P_0)} & \text{for } \Delta(\Omega, P_0) > 0 \\ 0 & \text{otherwise,} \end{cases} \quad (5)$$

where

$$\Delta(\Omega, P_0) := -P_0^2 \gamma_0^2 \tau_{\text{sh}}^2 \Omega^2 - P_0 2\gamma_0 \tilde{\beta}_e - \tilde{\beta}_e^2. \quad (6)$$

Since there is MI gain if, and only if,  $\Delta(\Omega, P_0) > 0$ , we may define the *MI gain region* in the  $\Omega - P_0$  plane as

$$R_{\text{MI}} = \{(\Omega, P_0) \in \mathbb{R} \times \mathbb{R}^+ : \Delta(\Omega, P_0) > 0\}. \quad (7)$$

Notice that for  $\tau_{\text{sh}} = 0$ , we get the usual textbook expression [19]

$$R_{\text{MI}}|_{\tau_{\text{sh}}=0} = \left\{ (\Omega, P_0) \in \mathbb{R} \times \mathbb{R}^+ : \begin{array}{l} \tilde{\beta}_e(\Omega) < 0, \\ P_0 > -\frac{\tilde{\beta}_e(\Omega)}{2\gamma_0} \end{array} \right\},$$

though we are interested in the case where self-steepening is not neglected, *i.e.*,  $\tau_{\text{sh}} \neq 0$ . Here,  $\Delta(\Omega, P_0) = 0$  defines the boundary of  $R_{\text{MI}}$  and is either met when  $\Omega = 0$  or whenever  $P_0$  is

$$P_{\pm} = \hat{P}(\Omega) \times \left( 1 \pm \sqrt{1 - \tau_{\text{sh}}^2 \Omega^2} \right), \quad (8)$$

where

$$\hat{P}(\Omega) = -\frac{\tilde{\beta}_e(\Omega)}{\gamma_0 \tau_{\text{sh}}^2 \Omega^2}. \quad (9)$$

Since for each fixed frequency  $\partial_{P_0}^2 \Delta(\Omega, P_0) < 0$ , it is clear that  $\Delta(\Omega, P_0)$  can only be positive between  $P_-$  and  $P_+$  when  $|\Omega| < \tau_{\text{sh}}^{-1}$ . It is usual to use the approximation  $\tau_{\text{sh}}^{-1} \approx \omega_0$ , thus neglecting the frequency dependence of the mode effective area [22]. In this case, Eq. (8) limits the frequency to lie in the range

$\Omega \in (-\omega_0, \omega_0)$ , whereas by taking into account the frequency dependence leads to a slightly increased value of  $\tau_{\text{sh}}$  and, hence, to a narrower range of frequencies where the MI gain exists (Ref. [23]).

From Eqs. (7)-(9), we can write

$$R_{\text{MI}} = \left\{ (\Omega, P_0) \in [-\omega_0, \omega_0] \times \mathbb{R}^+ : \tilde{\beta}_e(\Omega) < 0, \left( \frac{P_0}{\hat{P}(\Omega)} - 1 \right)^2 + (\tau_{\text{sh}}\Omega)^2 < 1 \right\}. \quad (10)$$

The  $R_{\text{MI}}$  of Eq. (10) has a direct *geometrical interpretation*: since  $1 \pm \sqrt{1 - \tau_{\text{sh}}^2 \Omega^2}$  defines an ellipse centered at  $(0, 1)$  with vertical axis of length 2 and horizontal axis of length  $2\omega_0$ , the MI gain region is given by the portion that lies above the  $P_0 = 0$  axis of the aforementioned ellipse, bent and stretched along the vertical axis by  $-\tilde{\beta}_e(\Omega)/(\gamma_0 \tau_{\text{sh}}^2 \Omega^2)$ . To see this, in Fig. 1 we plot MI gain regions in a plane of normalized power  $(P_0 \gamma_0 \tau_{\text{sh}}^2)$  versus frequency  $(\Omega)$  for  $\tilde{\beta}_e(\Omega) = (\beta_2/2)\Omega^2 + (\beta_4/4!)\Omega^4$  with  $\beta_2 = -1 \text{ ps}^2/\text{km}$ ,  $\beta_4$  taking on the values  $-0.8, 0, +0.8 \times 10^{-3} \text{ ps}^4/\text{km}$ , and  $\gamma_0 = 100 \text{ (W-km)}^{-1}$  with a pump centered at a wavelength of  $5 \mu\text{m}$ . Self-steepening is considered by setting  $\tau_{\text{sh}} = \omega_0^{-1}$ . The curves  $\tilde{\beta}_e(\Omega)/\Omega^2$  are also plotted as a reference.

With this interpretation in mind we can explain, for instance, the non-trivial behavior of the power cutoff above which MI gain nearly vanishes (but for the vestigial contribution due to the delayed Raman response.) Figure 2 shows the MI gain in the  $\Omega$ - $P_0$  plane using the same parameters of Fig. 1 but for  $\beta_4 = -1.6, -0.8, +0.8, +1.6 \times 10^{-3} \text{ ps}^4/\text{km}$  and with the addition of the delayed Raman response to show its negligible contribution to the shape of the MI gain region. The Raman response is  $R(T) = (1 - f_R)\delta(T) + f_R h_R(T)$ , with

$$h_R(T) = \frac{\tau_1^2 + \tau_2^2}{\tau_1 \tau_2^2} e^{-T/\tau_2} \sin(T/\tau_1) u(T), \quad (11)$$

where  $u(T)$  is the Heaviside step function,  $f_R = 0.031$ ,  $\tau_1 = 15.5 \text{ fs}$ ,  $\tau_2 = 230.5 \text{ fs}$  [24, 25, 26].

To see what happens with the power cutoff, Fig. 3 shows the pump power above which MI gain nearly vanishes as a function of  $\beta_4$  for 20 different values ranging from  $-1.6$  to  $+1.6 \times 10^{-3} \text{ ps}^4/\text{km}$  (the  $\beta_4$ 's of Fig. 2 are marked in red dots.) As it is readily seen, the cutoff power varies linearly with  $\beta_4$  for  $\beta_4 < 0$  and exhibits a *plateau* when  $\beta_4$  contributes towards the normal dispersion regime (that is,  $\beta_4 > 0$ ).

To explain the *plateau*, note that whenever  $\beta_4$  is positive the ellipse 'bends down', and therefore the power cutoff remains constant and equal to  $-\beta_2/(\gamma_0 \tau_{\text{sh}}^2)$  (*i.e.*,  $P_+$  for  $\Omega \rightarrow 0$ ). When  $\beta_4$  is negative, if  $|\beta_4|$  is not too small, the cutoff power (upper limit of the region along the vertical axis) lies near the position of the maxima of  $-\tilde{\beta}_e(\Omega)/\Omega^2$ , and it is easily seen that these maxima vary linearly

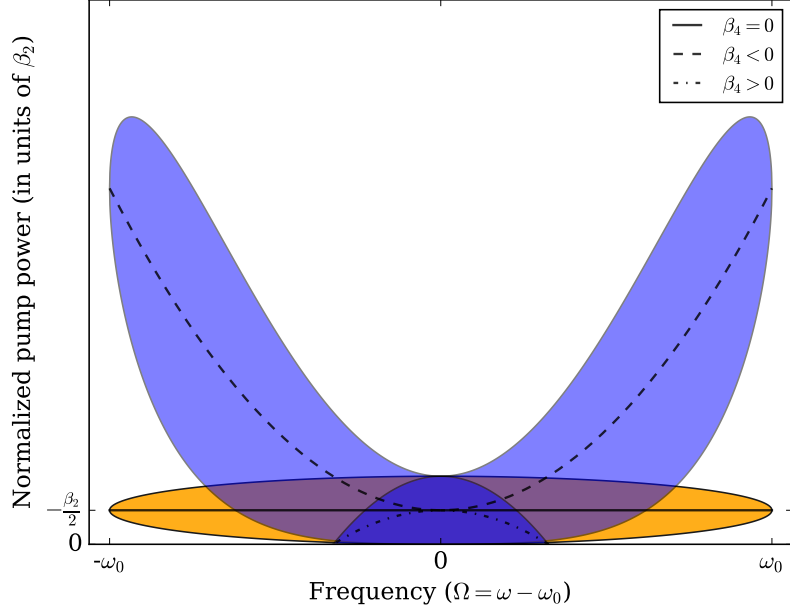


Figure 1: MI gain regions in the plane of normalized pump power versus frequency for  $\beta_4$  -0.8, 0, +0.8  $\times 10^{-3}$  ps<sup>4</sup>/km. Lines correspond to  $\tilde{\beta}_e(\Omega)/\Omega^2$ .

with  $\beta_4$ , explaining the approximately linear behavior seen in Fig. 3 for negative  $\beta_4$ 's.

All in all, the most obvious and important property that can be exploited from the geometrical description of the MI region is that, since the horizontal axis of the ellipse bends with  $-\tilde{\beta}_e(\Omega)/\Omega^2$ , one is able to synthesize different MI gain regions by the arbitrary design of the dispersion profile of the medium in a straightforward manner.

## 4 Location of the MI gain maxima

We may ask for the location of maxima within the MI gain region as it is paramount to applications which rely upon MI, such as supercontinuum generation from CW lasers and parametric amplification in nonlinear media. In order to do so, we find that

$$\partial_{P_0}\Delta = -2P_0\tau_{\text{sh}}^2\gamma_0^2\Omega^2 - 2\gamma_0\tilde{\beta}_e, \quad (12)$$

$$\partial_{P_0}^2\Delta = -2\tau_{\text{sh}}^2\gamma_0^2\Omega^2. \quad (13)$$

Since  $\partial_{P_0}^2\Delta$  is negative definite for  $\Omega \neq 0$ , by finding zeroes of Eq. (12) any maximum inside the MI gain region must have  $P_0 = -\tilde{\beta}_e(\Omega)/\gamma_0\tau_{\text{sh}}^2\Omega^2 = \hat{P}(\Omega)$ .

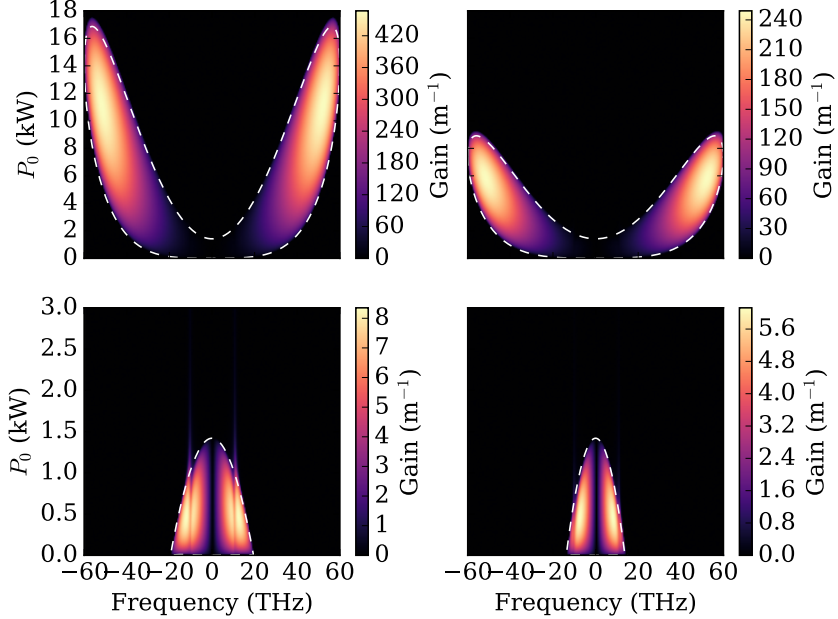


Figure 2: MI gain versus pump power when considering dispersion up to  $\beta_4 = -1.6, -0.8, +0.8, +1.6 \times 10^{-3} \text{ ps}^4/\text{km}$  (top left, top right, bottom left, and bottom right, respectively) including self-steepening. The corresponding MI gain regions are plotted in dashed white.

That is, maxima of the modulation instability gain must lie on the lines drawn in Fig. 1.

We may find the location of maxima by differentiating  $\Delta(\Omega, P_0)$  with respect to  $\Omega$  and proceeding with usual calculus techniques. However, a more intuitive understanding can be reached by defining

$$\begin{aligned} \hat{g}(\Omega) &:= \max_{P_0} g(\Omega, P_0) = g(\Omega, \hat{P}(\Omega)) \\ &= -2 \frac{\tilde{\beta}_e(\Omega)}{\tau_{\text{sh}} |\Omega|} \sqrt{1 - \tau_{\text{sh}}^2 \Omega^2} \end{aligned} \quad (14)$$

for  $\tilde{\beta}_e(\Omega) < 0$ . It is easy to see that maxima of  $g(\Omega, P_0)$  must also be maxima of  $\hat{g}(\Omega)$ .

By using Eq. (14) it can be easily shown that the location of maxima is  $\Omega_{\text{max}} = \pm 1/2\tau_{\text{sh}}$  and  $P_0 = -\frac{\beta_2}{2\gamma_0\tau_{\text{sh}}^2}$  for the simple case where only GVD is considered. That is, a peak in the MI gain right in the middle of the power range for which there is gain. This observation was first reported by Shukla and Rasmuseen [17]. However, the analysis in Ref. [17] did not include higher-order

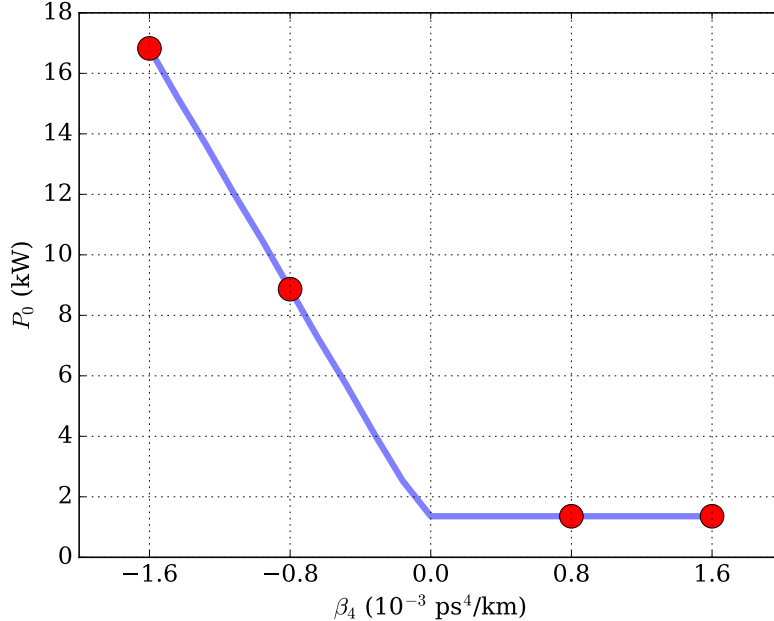


Figure 3: MI gain power cutoff versus  $\beta_4$ . Dots indicate the values of  $\beta_4$  used in previous figure.

dispersion terms. Thus, if we turn our attention to the influence of these terms, finding MI gain maxima and their location in the  $\Omega$ - $P_0$  plane, which amounts to a simple calculus problem by means of  $\partial_\Omega \hat{g}$  and  $\partial_\Omega^2 \hat{g}$ , gives us results which depend parametrically on the dispersion coefficients, and render the analysis (and synthesis) of extrema a straightforward numerical task.

As a simple example, we may consider analyzing the influence of  $\beta_4$  in MI gain maxima. If we define  $\hat{g}_{\beta_2}(\Omega)$  to be that of Eq. (14) when only GVD is considered, we have that

$$\hat{g}(\Omega_{\max}) = \hat{g}_{\beta_2}(\Omega_{\max}) + \partial_{\beta_4} \hat{g}(\Omega_{\max}) \cdot \beta_4$$

given that  $\tilde{\beta}_e(\Omega) < 0$ ,  $\beta_n = 0$  for  $n \geq 6$ , where  $\pm\Omega_{\max}$  are the arguments that maximize  $\hat{g}(\Omega)$ . In general,  $\Omega_{\max}$  depends on the particular dispersion profile, but it can be shown that, for  $|\beta_4|$  large enough,  $\Omega_{\max}$  remains nearly constant and  $\partial_{\beta_4} \hat{g}(\Omega_{\max})$  also varies little. In practical terms, this means that the gain increase over  $\hat{g}_{\beta_2}(\Omega_{\max})$  is proportional to  $|\beta_4|$ , thus pointing at the strong influence of high-order dispersion (see top left and top right panes of Fig. 2 and note the different scales.)

## 5 Conclusions

In conclusion, we presented a simple geometrical description of a full model of scalar modulation instability. This novel approach allowed us to relate the MI gain profile to any arbitrary dispersion of the medium, and provides a straightforward explanation of the dependence of the cutoff power with high-order dispersion. Further, we showed that the power level maximizing the MI gain is greatly influenced by high-order dispersion and that it can be explicitly obtained. Finally, the geometrical model can turn into a powerful tool to synthesize a desired MI gain shape with the potential application to a number of parametric-amplification and supercontinuum-generation devices that rely on a precise knowledge of MI dynamics.

## References

- [1] A. Hasegawa and W. Brinkman. Tunable coherent ir and fir sources utilizing modulation instability. *IEEE Journal of Quantum Electronics*, 16(7):694–697, Jul 1980.
- [2] D. Anderson and M. Lisak. Modulational instability of coherent optical-fiber transmission signals. *Opt. Lett.*, 9(10):468–470, Oct 1984.
- [3] K. Tai, A. Hasegawa, and A. Tomita. Observation of modulational instability in optical fibers. *Phys. Rev. Lett.*, 56:135–138, Jan 1986.
- [4] M. J. Potasek. Modulation instability in an extended nonlinear schrödinger equation. *Opt. Lett.*, 12(11):921–923, Nov 1987.
- [5] M. J. Potasek and G. P. Agrawal. Self-amplitude-modulation of optical pulses in nonlinear dispersive fibers. *Phys. Rev. A*, 36:3862–3867, Oct 1987.
- [6] Masataka Nakazawa, Kazunori Suzuki, Hirokazu Kubota, and Hermann A. Haus. High-order solitons and the modulational instability. *Phys. Rev. A*, 39:5768–5776, Jun 1989.
- [7] G. P. Agrawal. Modulation instability in erbium-doped fiber amplifiers. *IEEE Photonics Technology Letters*, 4(6):562–564, June 1992.
- [8] Ayhan Demircan and Uwe Bandelow. Supercontinuum generation by the modulation instability. *Optics communications*, 244(1):181–185, 2005.
- [9] Michael H. Frosz, Ole Bang, and Anders Bjarklev. Soliton collision and raman gain regimes in continuous-wave pumped supercontinuum generation. *Opt. Express*, 14(20):9391–9407, Oct 2006.
- [10] Michael H. Frosz, Thorkild Sørensen, and Ole Bang. Nanoengineering of photonic crystal fibers for supercontinuum spectral shaping. *J. Opt. Soc. Am. B*, 23(8):1692–1699, Aug 2006.

- [11] J. M. Dudley, G. Genty, F. Dias, B. Kibler, and N. Akhmediev. Modulation instability, akhmediev breathers and continuous wave supercontinuum generation. *Opt. Express*, 17(24):21497–21508, Nov 2009.
- [12] Martin E. Masip, A. A. Rieznik, Pablo G. König, Diego F. Grosz, Andrea V. Bragas, and Oscar E. Martinez. Femtosecond soliton source with fast and broad spectral tunability. *Opt. Lett.*, 34(6):842–844, Mar 2009.
- [13] K. Hammani, C. Finot, B. Kibler, and G. Millot. Soliton generation and rogue-wave-like behavior through fourth-order scalar modulation instability. *Photonics Journal, IEEE*, 1(3):205–212, Sept 2009.
- [14] Simon Toft Sørensen, Casper Larsen, Uffe Møller, Peter M. Moselund, Carsten L. Thomsen, and Ole Bang. Influence of pump power and modulation instability gain spectrum on seeded supercontinuum and rogue wave generation. *J. Opt. Soc. Am. B*, 29(10):2875–2885, Oct 2012.
- [15] Shanti Toenger, Thomas Godin, Cyril Billet, Frédéric Dias, Miro Erkintalo, Goëry Genty, and John M Dudley. Emergent rogue wave structures and statistics in spontaneous modulation instability. *Scientific reports*, 5, 2015.
- [16] J. Bonetti, S. M. Hernandez, P. I. Fierens, and D. F. Grosz. Analytical study of coherence in seeded modulation instability. *Phys. Rev. A*, 94:033826, Sep 2016.
- [17] P. K. Shukla and J. Juul Rasmussen. Modulational instability of short pulses in long optical fibers. *Opt. Lett.*, 11(3):171–173, Mar 1986.
- [18] Costantino De Angelis, Gianfranco Nalessi, and Marco Santagiustina. Role of nonlinear dispersion in the dynamics of induced modulational instability in kerr media. *J. Opt. Soc. Am. B*, 13(5):848–855, May 1996.
- [19] Govind Agrawal. *Nonlinear Fiber Optics*. Optics and Photonics. Academic Press, fifth edition, 2012.
- [20] F.Kh. Abdullaev, S.A. Darmanyan, S. Bischoff, P.L. Christiansen, and M.P. Sørensen. Modulational instability in optical fibers near the zero dispersion point. *Optics Communications*, 108(1 - 3):60 – 64, 1994.
- [21] F. Kh. Abdullaev, S. A. Darmanyan, S. Bischoff, and M. P. Sørensen. Modulational instability of electromagnetic waves in media with varying nonlinearity. *JOSA B*, 14(1):27–33, 1997.
- [22] K.J. Blow and D. Wood. Theoretical description of transient stimulated raman scattering in optical fibers. *IEEE Journal of Quantum Electronics*, 25(12):2665–2673, Dec 1989.
- [23] B. Kibler, J. M. Dudley, and S. Coen. Supercontinuum generation and nonlinear pulse propagation in photonic crystal fiber: influence of the frequency-dependent effective mode area. *Applied Physics B*, 81(2):337–342, 2005.

- [24] C. Xiong, E. Magi, F. Luan, A. Tuniz, S. Dekker, J. S. Sanghera, L. B. Shaw, I. D. Aggarwal, and B. J. Eggleton. Characterization of picosecond pulse nonlinear propagation in chalcogenide  $\text{As}_2\text{S}_3$  fiber. *Appl. Opt.*, 48(29):5467–5474, Oct 2009.
- [25] N. Granzow, S. P. Stark, M. A. Schmidt, A. S. Tverjanovich, L. Wondraczek, and P. St.J. Russell. Supercontinuum generation in chalcogenide-silica step-index fibers. *Opt. Express*, 19(21):21003–21010, Oct 2011.
- [26] M. R. Karim, B. M. A. Rahman, and Govind P. Agrawal. Mid-infrared supercontinuum generation using dispersion-engineered  $\text{Ge}_{11.5}\text{As}_{24}\text{Se}_{64.5}$  chalcogenide channel waveguide. *Opt. Express*, 23(5):6903–6914, Mar 2015.